Implantation sites of In, Cd, and Hf ions in diamond

K. Bharuth-Ram*
Physics Department, University of Durban-Westville, Durban 4000, South Africa

A. Burchard, M. Deicher, H. Quintel, and M. Restle
Fachbereich Physik, Universität Konstanz, D-78457 Konstanz, Germany

H. Hofsäss and C. Ronning
Zweites Physikalisches Institut, Universität Göttingen, D-37073 Göttingen, Germany
(Received 2 February 2001; revised manuscript received 13 June 2001; published 22 October 2001)

The implantation sites of In, Cd, and Hf ions in diamond have been investigated with complementary electron emission channeling (EC) and perturbed γ-γ angular correlations (PAC) spectrometry on radioactive ^{111}In, ^{111m}Cd, and ^{181}Hf probes implanted into natural type-IIa diamonds. The fraction of probes occupying specific sites were determined from comparisons of the measured axial channeling yields with channeling patterns calculated using the many-beam formalism of electron motion through the crystal. For the In-implanted sample the EC measurements, after room-temperature implantation and annealing at 1473 K or after implantation at 1373 K, show a substitutional or near-substitutional fraction of 32(4)%, a tetrahedral interstitial fraction of 10(3)%, and the remainder in highly disturbed environments. The γ-γ PAC measurements confirm the near-substitutional population, but show that about 10% of the In probes are at sites with nearest-neighbor point defects and 20% at sites with more distant defects, but none in a defect-free environment. The ^{111m}Cd measurements confirm these results and show that the loss of anisotropy in the PAC signal is not due to ''aftereffects'' of the electron capture decay of In to Cd, but due to extended lattice damage produced by the implantation process. The In PAC measurements confirmed the previously observed In-defect interaction in diamond, with a quadrupole coupling frequency of $\nu_Q = 117$ MHz, and in addition, showed evidence of a new defect interaction with $\nu_Q = 315$ MHz at annealing temperatures above 1473 K. A diamond sample implanted with overlapping profiles of ^{111}In and hydrogen and annealed up to 1673 K showed no evidence of the higher-frequency component or of any signal attributable to the formation of In-H pairs. This suggests that in diamond no significant fraction of the implanted In atoms act as electrically active acceptors. In the ^{181}Hf-implanted diamond, the present EC and PAC measurements yield consistent results of a near-substitutional fraction of only 10%–15%, in contrast to earlier observations.

DOI: 10.1103/PhysRevB.64.195207 PACS number(s): 61.80.Jh, 68.55.Ln, 81.20.−n

I. INTRODUCTION

Considerable research activity in the past two decades has been focused on ion implantation studies in diamond (see, for example, Refs. 1–17). This has been stimulated by some of the extreme properties of diamond, such as its wide band gap (5.4 eV), high thermal conductivity and hardness, and high mobility for both *p*- and *n*-type carriers, which make it potentially an ideal base for the fabrication of semiconducting devices. To realize this potential the problems of incorporating suitable dopants in the diamond lattice must be overcome.

Among the natural diamonds the type-IIb diamonds are *p*-type semiconducting, due to low levels of boron which forms an acceptor level at 0.37 eV above the top of the valence band.[7,18] Boron implantation of other natural and synthetic diamonds has also been shown to result in *p*-type conductivity.[6,16,17] Attempts at producing *n*-type semiconducting diamond layers have met with less success. Theoretical calculations show that, except for nitrogen, the formation energy of potential dopants is high (5.5 eV for Li, 10.4 eV for P, 15.3 eV for Na).[19] This and the metastable nature of the diamond structure preclude thermal diffusion as a means of incorporating the dopant atoms in the lattice. Ion implantation, which offers accurate control of dopant concentration and depth, is an attractive alternative. For a dopant atom to be electrically active it must rest at a regular lattice site in an unperturbed environment. Hence any damage of the lattice accompanying the implantation process must be annealed out and the lattice restored on a long-range scale. Several different implantation conditions and annealing procedures have been followed in this quest. These include implantation at low or room temperature and isochronal annealing, implantation at high temperature, and more recently cold implantation and rapid annealing (CIRA).[7]

Rutherford backscattering and channeling measurements[3] on ^{121}Sb, ^{74}Ge, ^{75}As, ^{31}P, and ^{6}Li implanted in diamond at high temperature (1373 K) show that substitutional fractions of about 50% can be achieved for Ge and As ions, while the Sb ions are randomly distributed in the lattice. Emission channeling studies by Hofsäss and co-workers[10–13] show that with conventional low dose implantation and annealing above 1270 K, substitutional fractions of 55% can be achieved for ^{73}As, 70% for ^{33}P, and 35% for ^{111}In, while ^{8}Li occupies both substitutional and tetrahedral interstitial sites.[14] These results show that ion implantation does achieve the required dopant concentrations, but leaves unanswered questions on the microstructure of the lattice in the vicinity of the implanted atoms.

In this contribution we report on investigations on the nature of implantation sites of heavy ions in diamond in which the radioactive nuclides ^{111}In, ^{111m}Cd, and ^{181}Hf were used as probes. These nuclides are particularly suited to such a study since the channeling effects of the conversion electrons emitted in their decay provide unambiguous identification of the lattice sites of the ions, while perturbed angular correlation (PAC) spectroscopy using gamma rays emitted in their decay cascade yields information on electric field gradients and, hence, on the microstructure of the lattice in the neighborhood of the probes.

Earlier PAC measurements on In-implanted diamond[1,9] showed a very small fraction of the implanted probes at sites with a unique electric field gradient (EFG). The majority experienced a distribution of electric field gradients indicating the high density of lattice defects induced by the implantation process. Emission channeling (EC) measurements following low-dose implantation and annealing above 1200 K, on the other hand, showed substitutional In fractions of about 30%–35%.[10,11] For ^{181}Hf-implanted diamond, the observed PAC spectra showed less than 10% of probes at sites with well-defined EFG's.[4] However, reanalysis of earlier EC data showed, surprisingly, approximately 50% of substitutionally implanted probes and about 50% on tetrahedral interstitial sites.[20] The large difference in site fractions is difficult to reconcile. In the earlier investigations the PAC and EC measurements were performed at different times and on different sets of samples, with implantation conditions also not being identical. In the present study these inconsistencies are obviated by performing EC and PAC measurements in sequence on the same samples after implantation and annealing.

In ^{111}In PAC spectroscopy the actual measurements are made on γ-γ cascades from the daughter ^{111}Cd nuclide following electron capture decay of the radioactive parent. The electron capture decay process generates a complex distortion of the electron configuration close to the PAC probe, and the subsequent Auger electron emissions leave the probe ions in a highly ionized state. If recovery towards an undistorted electronic environment is not complete before the first γ quantum of the daughter is emitted, i.e., within a few 100 ps, the anisotropy of the second γ is reduced and the PAC signal is strongly damped. In order to check for any loss of anisotropy in the PAC signals due to such decay ''aftereffects'' a comparative PAC measurement was done in which the isotope ^{111m}Cd, instead of ^{111}In, was directly implanted into a diamond sample. PAC measurements were made on the gamma cascade emitted in the direct decay of the isomeric ^{111m}Cd state. Emission channeling measurements were also made on the conversion electrons emitted in this decay.

This work therefore presents the results of several sets of measurements.

(a) EC and PAC measurements were made on a diamond sample implanted with ^{111}In at room-temperature (RT) and then annealed at various temperatures up to 1673 K to study the lattice sites of the implanted atoms and study annealing characteristics of radiation-induced damage.

(b) EC and PAC measurements were made on a diamond sample after ^{111}In implantation at 1373 K to check whether high-temperature implantation yielded a higher substitutional fraction than conventional RT implantation followed by high-temperature annealing.

(c) The influence of ''after effects'' of the electron capture $^{111}\text{In}\rightarrow{}^{111}$Cd decay on the anisotropy in the ^{111}In PAC measurements was checked in comparative EC and PAC measurements on a diamond sample directly implanted with metastable ^{111m}Cd ions.

(d) In an attempt to identify the observed quadrupole coupling frequencies and to search for In-H defect formation PAC measurements were performed on a diamond sample implanted with overlapping profiles of ^{111}In and H.

(e) Finally, EC and PAC measurements were made on a sample implanted with ^{181}Hf so as to resolve the anomaly in the site fractions determined in earlier studies.

II. EXPERIMENTAL DETAILS

A. Principles of the experimental techniques

1. Emission channeling

Details of emission channeling measurements are described in Refs. 21 and 22. Radioactive probe nuclei are implanted into single-crystal samples, and the yield of emitted charged particles (α, β^+, β^-, or conversion electrons) is measured outside the sample as a function of angle relative to the different crystal axes and planes. In the case of electron emission, the electron wave functions for transverse motion are strongly localized at the minimum of the effective potential, i.e., along the atomic rows or planes. Hence, for electron-emitting atoms located at substitutional sites, channeled electrons are bound to the positively charged atomic rows and consequently, result in enhanced emission yields along all crystallographic axes. For emitter atoms located away from the atomic rows the channeling effects are reduced; for example, in the $\langle 110\rangle$ axial direction electrons emitted from interstitial sites are not bound in axial or planar potentials and produce a nearly isotropic distribution.

In order to obtain quantitative estimates of the fractions of implanted ions at the different lattice sites channeling patterns $\chi_{th}(\Theta,\Phi)$ for the conversion electrons are calculated, within the many-beam formalism, around the principal axial directions and fitted to the respective measured channeling spectrum $\chi_{expt}(\Theta,\Phi)$. The effects of dechanneling and thermal vibrations of the probe nuclei are taken into account as discussed in Refs. 21 and 22. The corresponding fit function is given by

$$\chi_{fit}(\Theta,\Phi)=\left[1+\left(\sum_i f_i\chi_{expt}(\Theta,\Phi)_i-1\right)\right].$$

Θ and Φ are the horizontal and vertical tilt angles with respect to the axial direction, and f_i represents the fraction of implanted probes at site i. The remainder ($f_R=1-\Sigma f_i$) is assumed to be on nonunique or irregular sites of low symmetry. Comparison of measured yields with combinations of site-sensitive simulated channeling spectra permits one to obtain estimates of the occupancy of the modeled lattice sites.

2. Perturbed angular correlations

Details of the perturbed angular correlation method are reviewed in Refs. 23–25; aspects relevant to the present measurements are highlighted here. In essence, γ-γ PAC measurements consist of implanting excited probe nuclei into a host material and measuring the angular correlation between the γ rays emitted in the decay of the probe state and those that populate the probe state. Information on the lattice sites of the probe is inferred from the perturbation of the γ-γ angular correlation produced by the hyperfine interactions between the quadrupole moment of the excited nuclear state and the electric field gradients at the implantation sites.

The EFG is described in terms of a traceless tensor which has three diagonal elements V_{xx}, V_{yy}, and V_{zz}, arranged according to $V_{xx} \leqslant V_{yy} \leqslant V_{zz}$. It is completely specified by the largest of its three components, V_{zz}, and the asymmetry parameter

$$\eta = (V_{xx} - V_{yy})/V_{zz}, \quad \text{with} \quad 0 \leqslant \eta \leqslant 1.$$

The quadrupole coupling constant $\nu_Q = (eQV_{zz})/h$, where Q is the nuclear quadrupole moment, represents the strength of the EFG and η expresses its deviation from axial symmetry. For spin 5/2 the quadrupole frequency is related to the precession frequency ω,

$$\nu_Q = (10/3\pi)\omega.$$

In γ-γ PAC measurements with a conventional four detector $(180^\circ, 90^\circ)$ geometry, 12 time spectra are collected. The spectra are characterized by the lifetime of the probe state and the perturbation frequencies at the sites of the implanted probes. In the analysis the count rates N are used to generate the ratio $R(t)$, which is defined by

$$R(t) = \frac{2y-2}{y+2} \approx A_{22}^{eff} G_{22}(t), \quad \text{with} \quad y = \frac{\left(\prod_{m=1}^{4} N_m(180^\circ, t) \right)^{1/4}}{\left(\prod_{n=1}^{8} N_n(90^\circ, t) \right)^{1/8}}. \tag{1}$$

A_{22}^{eff} is the effective γ-ray angular correlation coefficient and $G_{22}(t)$ the perturbation function. The experimental $R(t)$ function is then fitted with a theoretical perturbation function for different lattice sites:

$$R_{theor}(t) = A_{22}^{eff} \sum_i f_i G_{22}^i(\eta k_i \nu_Q t), \quad \sum_i f_i = 1. \tag{2}$$

Each implantation site i is characterized by the fraction f_i, of probes occupying the site, the quadrupole coupling frequency ν_{Qi}, and the asymmetry parameter η_i.

For static quadrupole interactions the perturbation function is given by[24]

$$G_{22}(t) = S_0 + \sum_{n=1}^{3} \exp(-1/2\sigma_n^2 t^2) S_n(\eta, k_i) \cos(\omega_n t). \tag{3}$$

The coefficients $S_n(\eta, \mathbf{k}_i)$ depend on the asymmetry parameter and the orientation of the EFG with respect to the detector geometry; the exponential term takes account of slight variations in the EFG (assumed to have a Gaussian distribution around a mean value with width σ) which results in a damping of the perturbation.

The probe atoms may be exposed to several different microscopic environments, each with its characteristic perturbation function. As discussed by Wichert *et al.*,[24] four distinct situations can arise.

(i) Probe nuclei in an unperturbed site of tetrahedral or cubic symmetry experience no electric field gradient (i.e., $V_{ZZ} = 0$). The corresponding $R(t)$ function (and the perturbation function) has a constant value, independent of time t:

$$G_{22}(t) = S_0 + S_n = 1. \tag{3a}$$

(ii) Probes in a site of cubic symmetry, but surrounded by distant defects, experience a distribution of EFG's about $\langle V_{ZZ} = 0 \rangle$. The $R(t)$ spectrum shows a slow exponential decay with a perturbation described by

$$G_{22}(t) = S_0 + \sum_{n=1}^{3} \exp(-1/2\sigma_n^2 t^2) S_n. \tag{3b}$$

(iii) A probe nucleus at a site with a point defect in a nearest-neighbor position experiences a unique EFG. For a static distribution of EFG's the $R(t)$ spectrum is given by Eq. (3) above.

(iv) For probes at sites with extended defects in many different configurations in the immediate neighborhood, the $R(t)$ signal is rapidly damped.

B. Measurements

Natural type-IIa diamonds with $\langle 110 \rangle$ surface orientation were used in all measurements. The ^{111}In ions were implanted at the ion implanter at the University of Konstanz, the ^{111m}Cd ions at the on-line isotope separator ISOLDE at CERN, Geneva, and the ^{181}Hf ions at the Institut für Strahlen- und Kernphysik, University of Bonn. All implantations were done at an angle of about 7° to the surface normal to avoid channelling effects. The implantation energies, temperatures, and doses, together with SRIM (Ref. 26) estimated mean implantation depths and peak concentrations, for the different ions are listed in Table I.

The properties of the relevant nuclear states in the three probes and the γ-γ transitions and conversion electron emissions utilized in the PAC and EC measurements are listed in Table II. The EC measurements were made with a three-axis goniometer. The diamond samples were annealed in vacuum for 10 min at temperatures up to 1673 K, using either evacuated quartz ampoules or a graphite heater. After each annealing the diamond sample was preoriented with the aid of Laue x-ray photographs and then mounted in the vacuum chamber of the goniometer. Conversion electron emission yields were measured along the $\langle 110 \rangle$, $\langle 100 \rangle$, and $\langle 111 \rangle$ crystallographic directions, with a Si surface barrier detector with an angle

TABLE I. Implantation energies, temperatures, doses, and mean depths and peak concentrations of the different ions implanted into diamond.

Ion	E_i keV	T_i (K)	Dose cm^{-2}	Depth $A°$	Concentration (cm^{-3})
^{111}In	120	300	5×10^{12}	325(65)	2.8×10^{18}
	120	1373	5×10^{12}	325(65)	2.8×10^{18}
^{111m}Cd	60	300	6×10^{11}	195(40)	6.0×10^{17}
^{181}Hf	70	300	3×10^{13}	195(30)	3.8×10^{19}
^{1}H	5	300	1×10^{15}	380(90)	5.0×10^{20}
			2×10^{15}		1.0×10^{21}

resolution of 0.12° for the In and Cd measurements and 0.25° for the Hf measurements.

γ-γ PAC measurements were made on each sample immediately after an EC measurement, using a coplanar geometry of four detectors at angles $\theta_D=90°$ and 180°. The experimental $R(t)$ spectrum for each measurement was generated from 12 time spectra as discussed above. As our primary aim was to extract information on the fraction of probes at different lattice sites, the measurements were done in ''polycrystalline'' geometry. The small single-crystal diamond was embedded at the center of a sphere which was randomly rotated, at the axial center of the detector geometry, in a flowing air stream. By thus averaging all the crystal orientations one measures polycrystalline $S_n(\eta,\mathbf{k}_i)$ coefficients and obviates the need to know the crystal orientation as well as the EFG orientation.

III. RESULTS AND DISCUSSION

A. Emission channeling measurements:

Axial channeling peaks are expected along the ⟨111⟩ and ⟨100⟩ directions for electron-emitting probe nuclei located either at substitutional (S) or tetrahedral interstitial (T) sites. Along the ⟨110⟩ axis, however, an S site yields a channeling maximum and a T site almost isotropic emission distribution.[21,22] Theoretical axial channeling patterns were calculated (as discussed above) for emitters at substitutional, tetrahedral interstitial, and hexagonal interstitial sites, as well as for displacements along the ⟨111⟩ axis in antibonding and bond-center directions. The site fractions f_i were then determined from fits to the experimental spectra. Figure 1 displays the channeling effects observed along the ⟨110⟩, ⟨100⟩, and ⟨111⟩ axial directions for the In-implanted sample, after annealing at 1473 K. The strong channeling peaks show that the diamond samples are not amorphized and that an appreciable fraction of the implanted ions are at, or close to, substitutional lattice sites. The best fit to the data along the ⟨110⟩ direction is represented by the solid line in Fig. 1(a) which is the calculated yield for a substitutional fraction $f_S=0.32(4)$, a tetrahedral interstitial fraction $f_T=0.10(3)$, and a fraction $f_R=0.58$ at sites of extended damage which gives an isotropic channeling distribution. A good fit is also obtained for fractions $f_S=0.31(4)$ and $f_R=0.69$, represented by the dotted line. The dashed line represents calculated yields for $f_S=0.32$ plus a fraction 0.50 of probes displaced along the ⟨111⟩ axial direction halfway towards

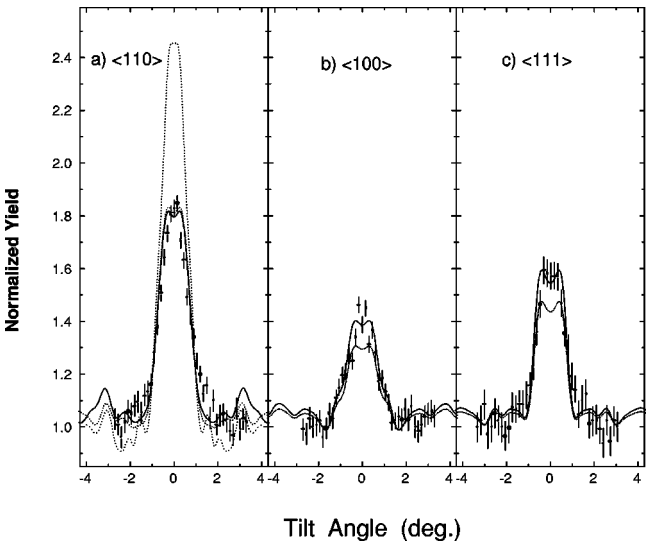

FIG. 1. Channeling spectra of conversion electrons emitted in the decay of ^{111}In implanted into diamond at 60 keV, observed along the three main axial directions. The lines represent calculated yields as discussed in the text.

TABLE II. Relevant nuclear properties of the ^{111}In (^{111}Cd), ^{111m}Cd and ^{181}Hf (^{181}Ta) probes, and the energies of the gamma rays and conversion electrons on which the PAC and EC measurements were made.

Probe	Transition	E_γ(keV)	$E_{K,L}$ (keV)	Q(b)	$T_{1/2}$
^{111}In→^{111}Cd*	$7/2^+\rightarrow5/2^+$	171.3	144.6 (K)		0.12 ns
			167.2 (L)		
	$5/2^+\rightarrow1/2^+$	245.4	218.7 (K)	0.77(12)	85.0 ns
			241.3 (L)		
^{111m}Cd	$11/2^+\rightarrow5/2^+$	150.8	124.1 (K)		48.5 ns
	$5/2^+\rightarrow1/2^+$	245.4	218.7 (K)	0.77(12)	85.0 ns
			241.3 (L)		
^{181}Hf→^{181}Ta*	$1/2^+\rightarrow5/2^+$	133.0	65.5 (K)		18μs
			121.3 (L)		
	$5/2^+\rightarrow7/2^+$	482.2		2.36(6)	10.8 ns

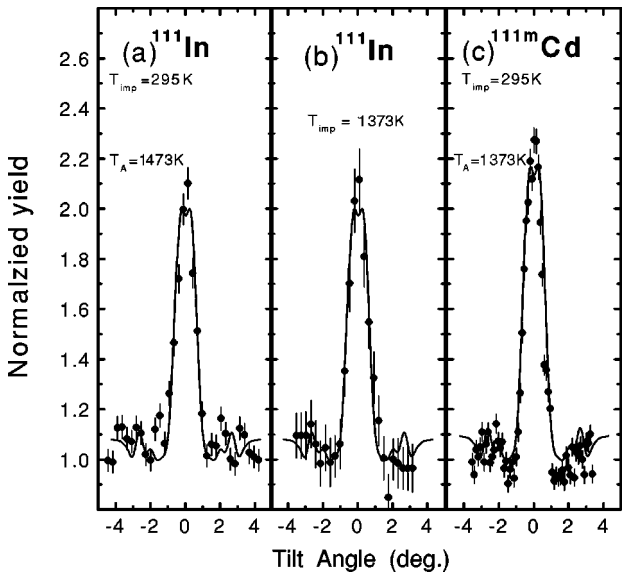

FIG. 2. Normalized channeling yields of conversion electrons emitted along the ⟨110⟩ axial direction (a) for ^{111}In implanted at sample temperature of 295 K and annealed at 1473 K, (b) for ^{111}In implanted at 1373 K, and (c) for ^{111m}Cd implanted at 295 K and sample annealed at 1373 K.

the bond center, as has been reported recently.[27] The channeling effects observed in our spectra are not consistent with such a large fraction of probes at such a configuration. The best fits along the ⟨100⟩ and ⟨111⟩ axial directions were obtained for substitutional fractions $f_S=0.42(4)$ and $f_S=0.40(4)$, respectively, with the remainder giving an isotropic distribution. The *S* and *T* sites are equivalent with respect to the channeling effects along these two axial directions. The channeling effects along all the three axial directions are thus consistent with a substitutional fraction of 32(4)%, an interstitial fraction of 10(3)%, and a random fraction $f_R=58\%$.

Figure 2 presents comparative channeling spectra in the ⟨110⟩ axial direction obtained for ^{111}In atoms implanted (a) at room temperature and annealed at 1273 K and (b) implanted at a sample temperature of 1373 K. The normalized yields are practically identical, showing that the same substitutional fractions can be achieved following either approach, i.e., room-temperature implantation followed by annealing above 1200 K or implantation at 1373 K.

B. PAC measurements

Figures 3 and 4 present the $R(t)$ spectra for the In and Cd implanted diamonds, together with their corresponding frequency spectra. The spectra for the In-implanted samples, after annealing or implantation at 1373 K [Fig. 3(a)], were identical. The fits to the spectra confirm the near-substitutional fraction observed in the EC measurements, but yield the following results on the microscopic nature of the probe sites.

(i) Practically none of the implanted probes are at defect-free sites.

(ii) 22(2)% of the probes show a slowly decaying $R(t)$ signal, reflecting their location as being one of tetrahedral or cubic symmetry but surrounded by distant defects.

(iii) 10(2)% of the probes experience a unique EFG due to In interactions at sites with nearest-neighbor point defects. After annealing at temperature $T_A=1373$ K, the quadrupole coupling frequency of this defect interaction is $\nu_Q=117(2)$ MHz and asymmetry $\eta=0.18$. After annealing at $T_A=1673$ K [Fig. 3(b)] only 2(1)% of the probes experience this EFG; the remaining 8% are at a new defect complex characterized by $\nu_Q=315(2)$ MHz and $\eta=0.86(3)$.

(iv) The vast majority (68%) of the probes experience a fast decay of the anisotropy, showing that they reside in sites with extended defects where they experience a distribution of EFG's.

Figure 3(c) shows the R(t) spectrum of the ^{111m}Cd-implanted sample after annealing the sample at 1473 K. The same strong attenuation of the signal is observed as

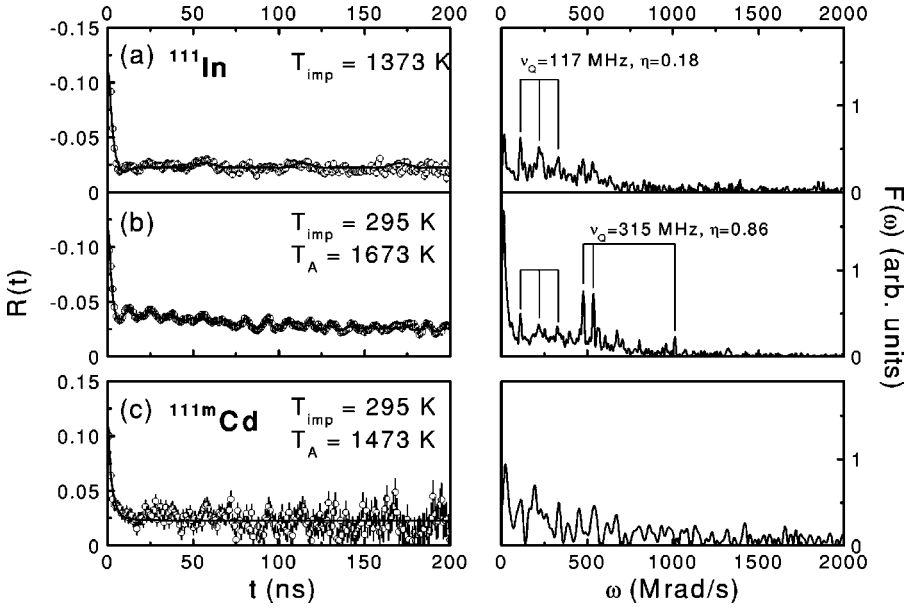

FIG. 3. $R(t)$ and frequency spectra of ^{111}In and ^{111m}Cd implanted in diamond at implantation and annealing temperatures indicated.

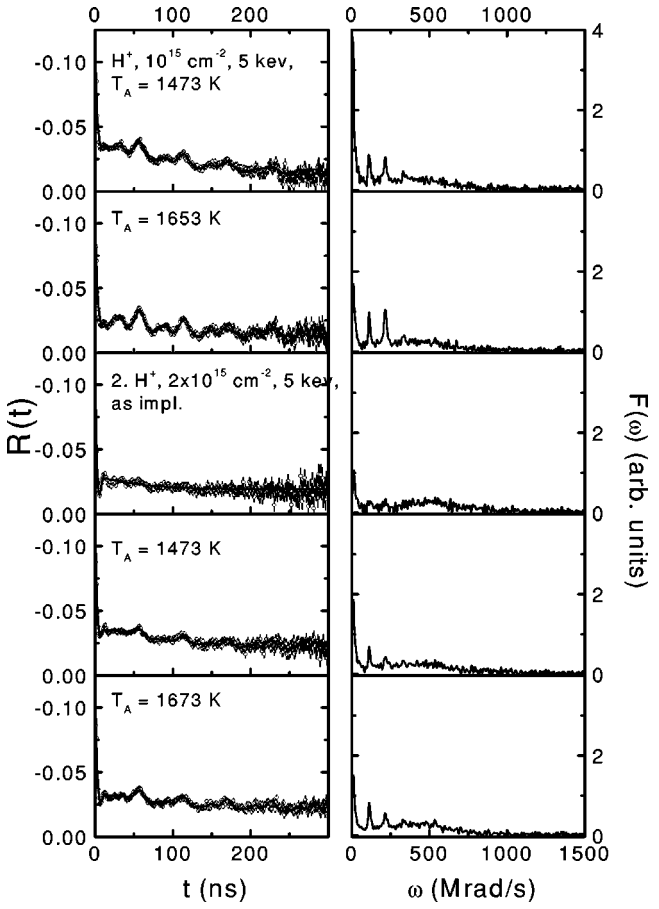

FIG. 4. $R(t)$ and frequency spectra of ^{111}In and H coimplanted in diamond.

for the In-implanted samples. No decay ''aftereffects'' come into play here, and only structural defects in the host lattice can be responsible for the strong attenuation. Evidently the annealing fails to remove the residual damage effects that follow the implantation process. The emission channeling pattern for this sample, displayed in Fig. 2(c), shows a significant channeling effect and indicates that the channeling effects on the emitted electrons are insensitive to low concentrations of nearest-neighbor defects.

The $R(t)$ and the frequency spectra for the diamond coimplanted with overlapping profiles of ^{111}In and H are displayed in Fig. 4, for the two implantation doses (1×10^{15} cm^{-2} and 2×10^{15} cm^{-2}) used in our investigations. The spectra after annealing at 1473 K and 1673 K are characterized only by a component with a quadrupole coupling frequency of $\nu_Q=117$ MHz, as has been observed in the In-implanted diamond (Fig. 3). There was no evidence of the 315 MHz signal, nor was there any evidence of any signal due to In-H complexes as has been observed in H-implanted Si (Refs. 28 and 29) and Ge (Ref. 30) formed by Coulombic attraction between the electrically active In and H.

Theoretical calculations of the lattice location of In in diamond, based on *ab initio* plane-wave pseudopotential theory, show the most stable site to be In in an off-center substitutional position, in between two carbon vacancies,

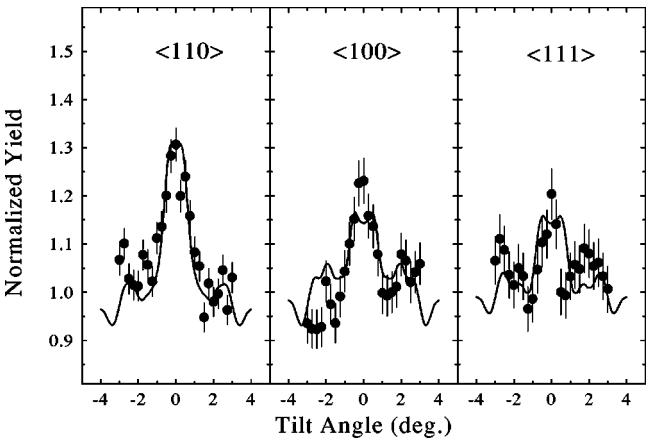

FIG. 5. Normalized channeling yields of conversion electrons emitted in the decay of ^{181}Hf implanted into diamond at 70 keV, observed along the three axial directions.

with an estimated quadrupole coupling frequency of approximately 100 MHz.[31] This value is in reasonable agreement with the observed frequency of 117 MHz.

C. ^{181}Hf in diamond

Figure 5 displays axial channeling spectra along the $\langle110\rangle$, $\langle100\rangle$, and $\langle111\rangle$ directions for the diamond sample implanted with ^{181}Hf at 300 K and annealed at 1673 K, while Fig. 6 presents the $R(t)$ spectra observed after annealing at 1473 K and 1673 K. The channeling effects are not very pronounced and correspond to near-substitutional fractions of 10%–14%, with the remainder on sites that give an isotropic emission distribution. The $R(t)$ spectra are consistent with this and the fit yields two sites with equal populations of 5(1)%, with quadrupole coupling frequencies of 335 MHz and 580 MHz, in agreement with the results of Raudies *et al.*[4] Comparing the results obtained after ^{111}In and ^{181}Hf implantation shows that after annealing above 1300 K more In than Hf atoms reside on substitutional lattice sites although their atomic radii are very similar. Theoretical studies on P and In implanted in diamond indicate strong binding energies of the implanted atoms with vacancies.[31,32] Hence the result that fewer Hf than In atoms are observed at substitutional sites is not unexpected as the vacancy concentration produced in diamond by 70 keV Hf ions is at least an order of magnitude higher than that produced by 120 keV In ions and is close to the amorphization threshold.

In summary, several experimental facts emerge from our EC and PAC measurements. For both the probe nuclei ^{111}In and ^{181}Hf, the two complimentary methods give consistent fractions of implanted probes close to substitutional sites in the diamond lattice. The PAC results, however, do not show any evidence of any defect-free annealing of the diamond lattice. The EC and PAC results of the ^{111}In-implanted sample rule out any large fraction of In atoms at a displaced S→BC site along the $\langle111\rangle$ axis, as has been reported recently by Doyle *et al.*[27] Such a configuration would give an axially symmetric electric field gradient with its principal axis along $\langle111\rangle$. A large fraction (50%) of probes at this

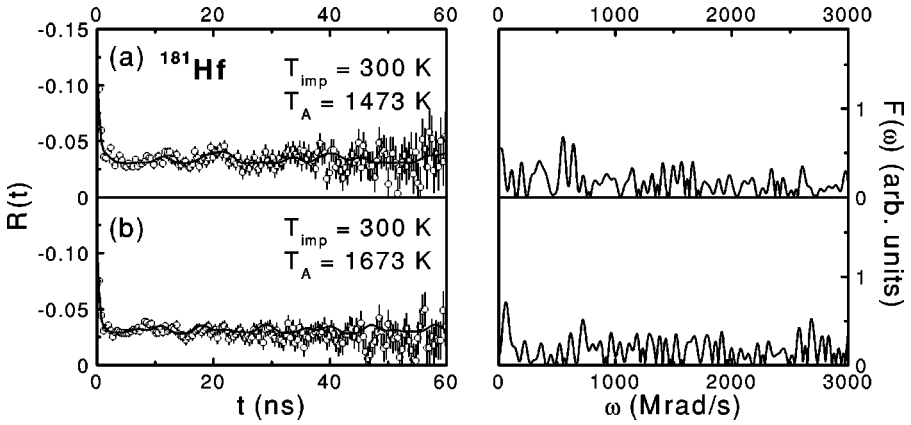

FIG. 6. $R(t)$ and frequency spectra of ^{181}Hf implanted in diamond at 300 K, after annealing at 1473 K and 1673 K.

site together with a 30% fraction of substitutional probes would yield an $R(t)$ spectrum with amplitude about a factor of 3 larger than observed in the present work as well as in previous studies.

The disappearance of the 315 MHz PAC signal in the hydrogen coimplanted diamond, after annealing at 1673 K, also merits comment. It is well established that ion implantation in diamond is accompanied by lattice damage due to the breaking up of some of its sp^3 bonds. Under appropriate conditions the broken bonds may reorganize to form stable sp^2 bonds and result in the formation of graphitized regions in the lattice. The damage density threshold beyond which graphitization occurs in diamond after annealing is 10^{22} vacancies/cm^3.[33] In our case, a total dose of 5×10^{12} cm^{-2} of 120 keV^{111}In ions is estimated (SRIM) to produced about 1.6×10^{21} vacancies/cm^3, which is below this threshold. A possible explanation of the 315 MHz signal observed at $T_A = 1673$ K is that it is due to In atoms attached to dangling C bonds at damaged regions in the diamond lattice. In the H-implanted sample these bonds may be terminated by the more mobile hydrogen atoms and are not available to the In atoms, resulting in the disappearance of the 315 MHz signal. The absence of any new EFG signal attributable to the formation of In-H pairs has an additional significance. Such pair formation is driven by the Coulombic attraction between the acceptor In and the H. This leads to the conclusion that in diamond no significant fraction of the implanted In atoms act as electrically active acceptors.

Finally, the $R(t)$ spectra of the ^{111}In- and ^{111m}Cd-implanted diamond samples display the same strong attenuation of the PAC signals, thus excluding decay aftereffects as the reason for the loss in γ-γ anisotropy and showing that the bulk of the implanted atoms are in strongly perturbed surroundings. Evidently, these implantation-induced defects do not disappear even at annealing temperatures as high as 1673 K.

IV. CONCLUSIONS

The emission channeling results show that appreciable fractions of ion-implanted atoms ($\approx$30% In and $\approx$10% Hf) at substitutional sites in diamond can be achieved either by annealing or implantation at high temperatures. In the case of In-implanted diamond, earlier EC results show two annealing stages, one setting in at about 600 K and the other at ing stages, one setting in at about 600 K and the other at 1200 K.[11] The present PAC measurements on the In- and Cd-implanted diamonds rule out decay after effects as the cause of the rapid loss of γ-ray anisotropy, but show, on the other hand, that even after annealing at temperatures as high as 1673 K residual lattice damage induced by the implantation process still remains and no defect-free restoration of the lattice is achieved, which is a prerequisite for the electrical activation of dopants. These results therefore beg the question: can incorporation of dopant atoms at defect-free sites in the diamond lattice be achieved by ion implantation? Direct evidence of the incorporation of small but appreciable fractions of atoms at defect-free sites in diamond comes from in-beam Mössbauer spectroscopy and β-NMR measurements on ^{57}Fe and ^{12}B, respectively, recoil implanted into diamond.[34,35] Characteristic of both these measurements is the broad kinematic spread in recoil energies, which result in a rather flat implantation profile with dopant concentrations several orders of magnitude lower than in conventional single-energy implantation methods. This suggests that to achieve dopant incorporation at defect-free, regular, lattice sites in diamond low-dose implantation at a range of energies is required.

The combined EC and PAC measurements presented here also caution against over-interpretation of the results of emission channeling measurements. In the theoretical simulations the emitter atoms are placed at the modeled sites in a perfect defect-free lattice. The comparison between the experimental and theoretical channeling effects thus allows one to identify whether the emitting atoms are located at substitutional or certain simple interstitial sites and, in favorable cases, on more complex configurations provided detailed information on lattice defects is available. However, information on the microstructure of the dopant sites requires complimentary measurements by techniques such as Mössbauer spectroscopy, PAC or nuclear magnetic resonance, and electrical and optical measurements.

ACKNOWLEDGMENTS

The authors thank Dr. K. Freitag of the Institut för Strahlen und Kernphysik, Universität Bonn, for the ^{181}Hf implantation. This work has been supported by the National Research Foundation (South Africa) and the Bundesminister für Bildung, Wissenschaft, Forschung und Technologie under Grant No. 03-De5KO1-6.

*Corresponding author. Electronic address: kbr@pixie.udw.ac.za

[1] R. Kalish, M. Deicher, E. Recknagel, and Th. Wichert, J. Appl. Phys. **50**, 6870 (1979).
[2] H. Appel, J. Raudies, W.-G. Thies, A Hanser, and J.P.F. Sellschop, Hyperfine Interact. **10**, 735 (1981).
[3] G. Braunstein and R. Kalish, J. Appl. Phys. **54**, 2106 (1983).
[4] J.H. Raudies, H. Appel, G.M. Then, and W.G. Thies, Hyperfine Interact. **15/16**, 483 (1983).
[5] J.P.F. Sellschop, S.H. Connell, K. Bharuth-Ram, H. Appel, E. Sideras-Haddad, and M. Stemmett, Mater. Sci. Eng., B **11**, 227 (1992).
[6] J. Prins, Phys. Rev. B **38**, 5576 (1988).
[7] J. Prins, Mater. Sci. Rep. **7**, 271 (1992).
[8] S. Prawer, C. Uzay-Saguy, G. Braunstein, and R. Kalish, Appl. Phys. Lett. **63**, 2502 (1993).
[9] A. Burchard, M. Restle, M. Deicher, H. Hofsäss, S.G. Jahn, Th. König, R. Magerle, W. Pfeiffer, and U. Wahl, Physica B **185**, 150 (1993).
[10] H. Hofsäss, M. Restle, U. Wahl, and E. Recknagel, Nucl. Instrum. Methods Phys. Res. B **80/81**, 176 (1993).
[11] H. Quintel, K. Bharuth-Ram, H. Hofsäss, M. Restle, and C. Ronning, Nucl. Instrum. Methods Phys. Res. B **118**, 72 (1993).
[12] K. Bharuth-Ram, H. Quintel, M. Restle, C. Ronning, H. Hofsäss, and S.G. Jahn, J. Appl. Phys. **78**, 5180 (1995).
[13] H. Hofsäss, M. Dalmer, M. Restle, and C. Ronning, J. Appl. Phys. **81**, 2566 (1997).
[14] M. Restle, K. Bharuth-Ram, H. Quintel, C. Ronning, and H. Hofsäss, Appl. Phys. Lett. **66**, 2733 (1995).
[15] S. Prawer and R. Kalish, Phys. Rev. B **51**, 15 711 (1995).
[16] R. Kalish, Appl. Surf. Sci. **117-118**, 558 (1997).
[17] R. Kalish, Carbon **37**, 781 (1999).
[18] R.M. Chrenko, Phys. Rev. B **7**, 4560 (1973).
[19] S.A. Kajihara, A. Antonelli, and J. Bernholc, Phys. Rev. Lett. **66**, 2010 (1991).
[20] E.J. Storbeck, S.H. Connell, J.P.F. Sellschop, and H. Hofsäss, Nucl. Instrum. Methods Phys. Res. B **85**, 503 (1994).
[21] H. Hofsäss and G. Lindner, Phys. Rep. **20**, 123 (1991).
[22] H. Hofsäss, Hyperfine Interact. **97/98**, 247 (1996).
[23] H. Frauenfelder and R. Steffen, in *Alpha-, Beta-, Gamma-ray Spectroscopy*, editd by K. Siegbahn (North-Holland, Amsterdam, 1965), Vol. 2, p. 997.
[24] Th. Wichert and E. Recknagel, in *Microscopic Methods in Metals*, edited by U. Gonser, Topics in Current Physics, Vol. 40 (Springer, Berlin, 1986), p. 317.
[25] Th. Wichert, M. Deicher, G. Grübel, R. Keller, N. Schultz, and H. Skudlik, Appl. Phys. A: Solids Surf. **48**, 59 (1989).
[26] J.F. Ziegler, J.P. Biersack, and U. Littmark, *The Stopping and Range of Ions in Solids* (Pergamon, New York, 1985).
[27] B.P. Doyle, E. Storbeck, U. Wahl, S.H. Connell, and J.P. Sellschop, J. Phys.: Condens. Matter **12**, 67 (2000).
[28] H. Skudlik, M. Deicher, R. Keller, R. Magerle, W. Pfeiffer, P. Pross, E. Recknagel, and Th. Wichert, Phys. Rev. B **46**, 2159 (1992).
[29] H. Skudlik, M. Deicher, R. Keller, R. Magerle, W. Pfeiffer, P. Pross, E. Recknagel, and Th. Wichert, Phys. Rev. B **46**, 2172 (1992).
[30] M. Deicher, R. Keller, W. Pfeiffer, H. Skudlik, and Th. Wichert, Physica B **170**, 335 (1991).
[31] B.P. Doyle, J.K. Dewhurst, J.E. Lowther, and K. Bharuth-Ram, Phys. Rev. B **57**, 4965 (1998).
[32] R. Jones, J.E. Lowther, and J. Goss, Appl. Phys. Lett. **69**, 2489 (1996).
[33] C. Uzan-Saguy, C. Cytermann, V. Richter, M. Shaanan, and R. Kalish, Appl. Phys. Lett. **67**, 1194 (1995).
[34] B. Ittermann *et al.*, Appl. Phys. Lett. **71**, 3658 (1997).
[35] K. Bharuth-Ram, M. Hartick, E. Kankeleit, C. Dorn, P. Held, R. Sielemann, L. Wende, and J.P.F. Sellschop, Phys. Rev. B **58**, 8955 (1998).